SAC Steel Project Building Models Development in OpenSees

Scope

The present document describes the three and 9-story SAC Steel Project buildings designed for Los Angeles and Seattle according to pre-Northridge codes and provides detailed information on the finite element models, which were developed in the Open System for Earthquake Engineering Simulation (OpenSees) platform, of these buildings. This models are used to study the tsunami fragility and sensitivity analysis through a surrogate modeling based methodology.

1 Building models

The steel moment resisting frame buildings studied in this work are a subset of the models developed as part of the SAC steel project (FEMA 2000) for Los Angeles and Seattle. The structures studied herein are the Los Angeles 3 and 9-story buildings and the Seattle 3-story building, denoted as LA3, LA9, and SEA3, respectively. The buildings, which were designed by using pre-Northridge codes (ICBO 1994), have external frames designed to resist the lateral seismic loads and interior frames designed as gravity frames. As shown in Figure 1 and Figure 2, all three buildings have 9.15 m spans in both directions. The height of the frames is constant and equal to 3.96 m, except for the basement and ground levels of the 9-story building (see Figure 2) which have heights of 3.65 m and 5.49 m, respectively. The shaded area in the plan views represents the penthouse location. Table 1 to Table 3 show the beam and column sections of both the perimeter moment resisting frame and the interior gravity frames, as well as Seattle's doubler plates thickness. A detailed description of the buildings is presented in FEMA 355C (2000) and Gupta and Krawinkler (1999).

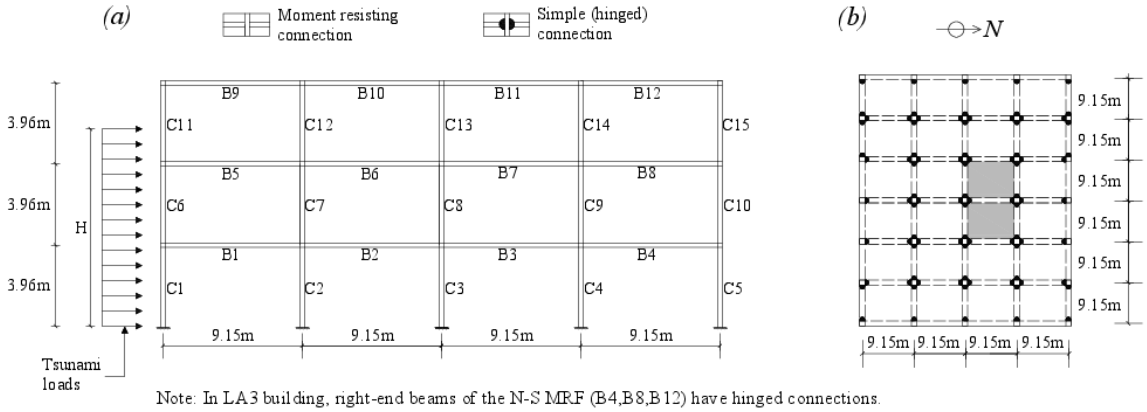

Figure 1 –3-Story steel moment frame buildings (LA3 and SEA3 buildings): (a) elevation of the SMRF in the NS direction (exterior frame); (b) plan view.

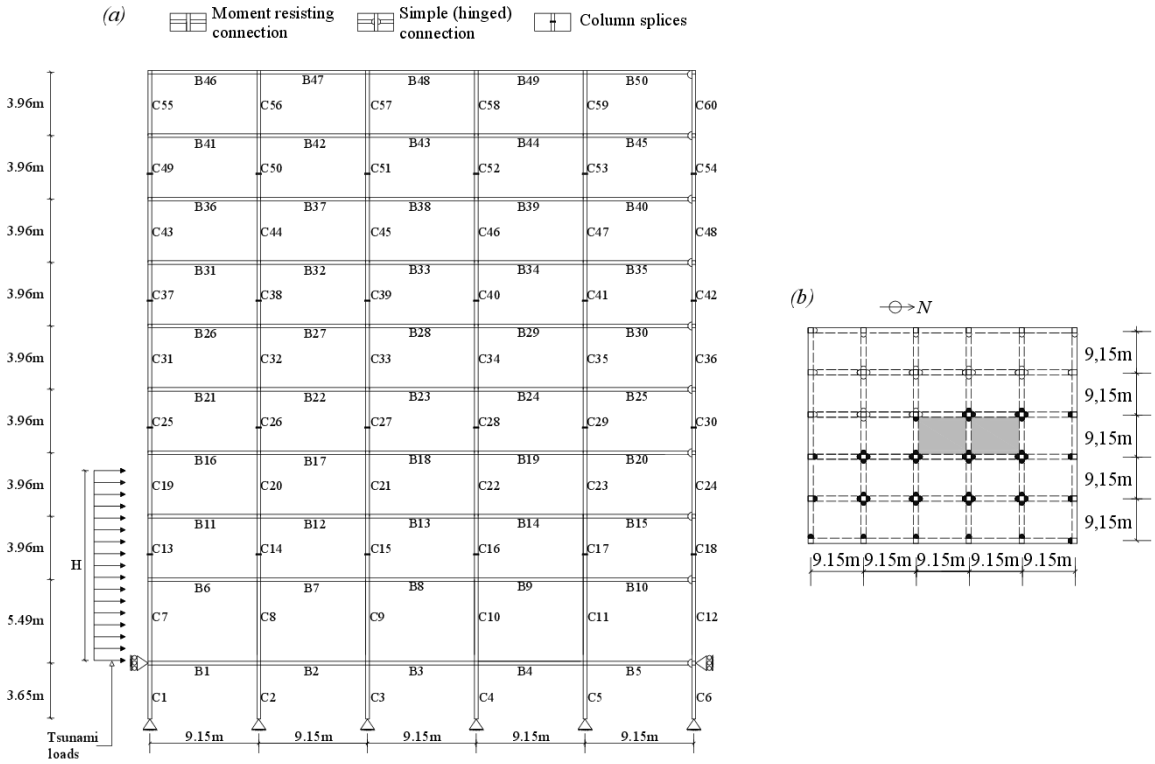

Figure 2 – Los Angeles 9-Story steel moment frame building (LA9 building): (a) elevation of the SMRF in the NS direction (exterior frame); (b) plan view.

Table 1 – Building column and beam sections (LA3 building)

Level	N-S Moment Resisting Frame			N-S Gravity Frames		
	Columns		Girder	Columns		Beams
	Exterior	Interior		Below penthouse	Others	
1	W14x257 (C1 & C5)	W14x311 (C2 – C4)	W33x118 (B1 – B4)	W14x82 (C3 & C4)	W14x68 (C1,C2 & C5)	W18x35 (B1 – B4)
2	W14x257 (C6 & C10)	W14x311 (C7 – C9)	W30x116 (B5 – B8)	W14x82 (C8 & C9)	W14x68 (C6,C7 & C10)	W18x35 (B5 – B8)
3	W14x257 (C11 & C15)	W14x311 (C12 – C14)	W24x68 (B9 – B12)	W14x82 (C13 & C14)	W14x68 (C11,C12 & C15)	W16x26 (B9 – B12)

Table 2 – Building column and beam sections (SEA3 building)

Level	N-S Moment Resisting Frame				N-S Gravity Frames	
	Columns		Girder	Doubler Plates (mm) Int./Ext.	Columns	Beams
	Exterior	Interior				
1	W14x159 (C1 & C5)	W14x176 (C2 – C4)	W24x76 (B1 – B4)	0 / 6.35	W10x77 (C1 - C5)	W18x35 (B1 – B4)

2	W14x159 (C6 & C10)	W14x176 (C7 – C9)	W24x84 (B5 – B8)	0 / 14.29	W10x77 / W10x60 (C6 - C10)	W18x35 (B5 – B8)
3	W14x159 (C11 & C15)	W14x176 (C12 – C14)	W18x40 (B9 – B12)	0 / 0	W10x60 (C11 - C15)	W16x26 (B9 – B12)

Table 3 – Building column and beam sections (LA9 building)

Level	N-S Moment Resisting Frame			N-S Gravity Frames		
	Columns		Girder	Columns		Beams
	Exterior	Interior		Below penthouse	Others	
-1	W14x370 (C1 & C6)	W14x500 (C2 – C5)	W36x160 (B1 – B5)	W14x211 (C3 – C5)	W14x193 (C1,C2 & C6)	W21x44 (B1 – B5)
1	W14x370 (C7 & C12)	W14x500 (C8 - C11)	W36x160 (B6 – B10)	W14x211 (C9 – C11)	W14x193 (C7,C8 & C12)	W18x35 (B6 – B10)
2	W14x370 / W14X370 (C13 & C18)	W14x500 / W14x455 (C14 - C17)	W36x160 (B11 – B15)	W14x211 / W14x159 (C15 – C17)	W14x193 / W14x145 (C13,C14 & C18)	W18x35 (B11 – B15)
3	W14x370 (C19 & C24)	W14x455 (C20 - C23)	W36x135 (B16 – B20)	W14x159 (C21 – C23)	W14x145 (C19,C20 & C24)	W18x35 (B16 – B20)
4	W14x370 / W14x283 (C25 & C30)	W14x455 / W14x370 (C26 – C29)	W36x135 (B21 – B25)	W14x159 / W14x120 (C27 – C29)	W14x145 / W14x109 (C25,C26 & C30)	W18x35 (B21 – B25)
5	W14x283 (C31 & C36)	W14x370 (C32 - C35)	W36x135 (B26 – B30)	W14x120 (C33 – C35)	W14x109 (C31,C32 & C36)	W18x35 (B26 – B30)
6	W14x283 / W14x257 (C37 & C42)	W14x370 / W14x283 (C38 - C41)	W36x135 (B31 – B35)	W14x120 / W14x90 (C39 – C41)	W14x109 / W14x82 (C37,C38 & C42)	W18x35 (B31 – B35)
7	W14x257 (C43 & C48)	W14x283 (C44 - C47)	W30x99 (B36 – B40)	W14x90 (C45 – C47)	W14x82 (C43,C44 & C48)	W18x35 (B36 – B40)
8	W14x257 / W14x233 (C49 & C54)	W14x283 / W14x257 (C50 - C53)	W27x84 (B41 – B45)	W14x90 / W14x61 (C51 – C53)	W14x82 / W14x48 (C49,C50 & C54)	W18x35 (B41 – B45)
9	W14x233 (C55 & C60)	W14x257 (C56 – C59)	W24x68 (B46 – B50)	W14x61 (C57 – C59)	W14x48 (C55,C56 & C60)	W16x26 (B46 – B50)

Notes:

- For the LA9 building, exterior columns on the right alignment (C6, C12, … , C60) are oriented about the weak axis.
- Columns divided by splices (indicated with a "/" in the tables) are modeled by assigning the smaller section to a single column element.

2 Numerical Models

2.1 Introduction

Two-dimensional models of the buildings are used for structural analysis and developed in the Open System for Earthquake Engineering Simulation (OpenSees, v2.5.0) platform. These models follow the approach in FEMA 355C (2000) in developing two different models, namely the M1 and M2A models. M1 models are basic centerline models of the bare moment resisting frame, whereas M2A models are considered to provide the most reasonable estimate of structure strength and stiffness by explicitly modeling secondary sources of strength and stiffness, namely panel zones, shear connections, floor slabs, and interior gravity frames. In both models, strong-column weak-beam ductile behavior was assumed for both models. A rigid diaphragm is assumed for each floor. Geometric nonlinearities are accounted for during the analysis by considering P-Δ geometric transformation at beams and columns of the moment resisting frame and the interior gravity frames (in model M2A), and a P-Δ leaning column in model M1. Brittle connection fracture modes and soil-structure interaction are not considered in these models. Masses are applied to beam-column joints, whereas loads are applied to both beam-columns joints and beam spanning in the N-S direction. Penthouse's weight (and mass) is considered at the building's roof.

Similar to the definition in FEMA 355C (2000), Rayleigh damping is assigned to the models. Following indications in Erduran (2012), a damping ratio of 2% is assigned to the period of vibration for the first mode and a higher mode when defining the Rayleigh damping model used. Following FEMA 355C (2000), the higher mode considered was one corresponding to a period of vibration of 0.2 sec (a period close to LA3's and SEA3's third modal period and LA9's fifth modal period). Herein, uncertainties are propagated in the yield strength of the columns and the beams by considering a lognormal distribution with 8% dispersion. In case of LA buildings, the median strength for columns and beams is 57.7 ksi and 49.2 ksi respectively. The median yield strength of columns and beams in the Seattle 3 story building is 57.7 ksi. According to the objectives of this work, the M1 model is only developed for the LA3 building, while M2A models are developed for LA3, SEA3, and LA9 buildings.

2.2 Modeling Approach

M1 model consists of a two-dimensional centerline model of one of the two (identical) N-S (North-South) perimeter moment resisting frames (MRF) of the building. Geometric nonlinearities are accounted for during the analysis by considering P-Δ geometric transformation at beams and columns of the moment resisting frame and a P-Δ leaning column. Otherwise, M2A model includes one of the N-S MRF and the tributary contribution to stiffness and strength of the following elements: (1) columns that form the orthogonal MRF; (2) interior (gravity) frames beams and columns; (3) panel zones strength and stiffness; (4) floor slabs stiffness contribution; and (5) simple (shear) connections strength and stiffness. The columns that form the orthogonal MRF and the interior gravity frames are modeled through an equivalent frame, designated as consolidated frame, attached to the MRF through rigid link elements. Shear connections are modeled by introducing a zero-length spring with limited strength and stiffness according to the methodology in FEMA 355c (2000). Furthermore, panel zone regions are modeled using a combination of rigid beam-column elastic elements, which form a parallelogram, and a zero-length rotational spring that simulates the trilinear shear-distortion relationship (Gupta and Krawinkler, 1999). Figure 3 and Figure 4 show a graphical representation of the M1 and M2A models, respectively, developed for the LA3 building.

Note that the interior gravity columns, which are modeled in the consolidated frame, contribute to the stiffness and strength of the building due to the imposed displacement compatibility, or in

other words since these columns have to follow the deflected shape of the moment frames. As a consequence, non-negligible shear forces may be generated. This is particularly true in the first story for structures with basements where columns continue to the base of the structure, resulting in identical boundary conditions for all columns (exterior and gravity columns) at ground level.

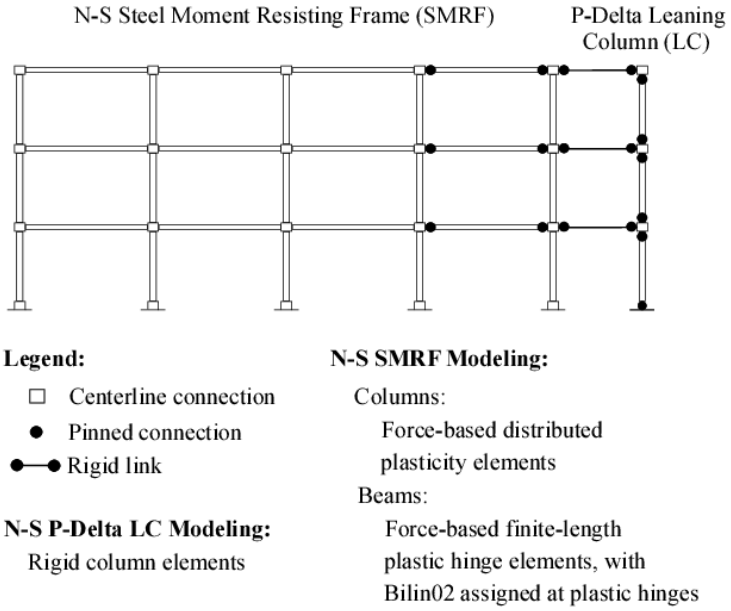

Figure 3 – Graphical representation of the M1 model for LA3 building.

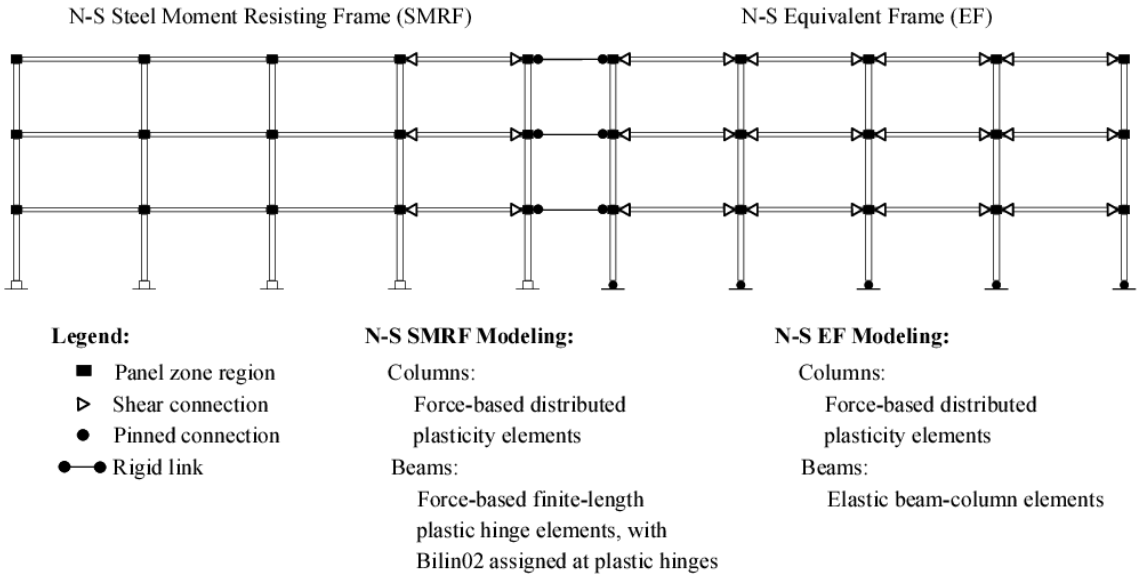

Figure 4 – Graphical representation of the M2A model for LA3 building.

The welded beam-to-column joints in this study are taken to be fully restrained joints, defined as joints that result in less than 5% contribution to the frame displacements (FEMA 273). Thus, the beam-to-column joints are assumed to have infinite strength and stiffness. Research on the

effects of brittle fracture around beam-to-column joint welds was developed by Cornel and Luco (2000), but are not considered herein.

The nonlinear behavior of the buildings was modeled considering two different approaches. The two approaches differ in the model used to simulate the beam moment-rotation nonlinear behavior. The two models consider a finite-length plastic hinge element based on a modified Radau integration scheme to simulate beam behavior (Scott and Fenves 2006, Ribeiro et al. 2015). However, the first model considers an elastic-plastic model with strain-hardening, therefore designated as MRSH (Modified Radau with Strain Hardening), while the second model employs a bilinear model with deterioration (Ribeiro, 2017), therefore designated as MRB (Modified Radau with Bilin). Table 4 summarizes the eight different models developed. All models consider force-based fiber section distributed plasticity elements to simulate column behavior.

Table 4 – Summary of the developed models

Building	Models			
	M1		M2A	
	MRB	MRSH	MRB	MRSH
LA3	✓	✓	✓	✓
SEA3			✓	✓
LA9			✓	✓

As mentioned above, the models developed in this work follow the general approach of the FEMA M2A models. The FEMA 355 models were developed in the DRAIN-2DX (Allahabadi and Powell, 1988) computer program. The main differences between the models developed herein using OpenSees and the FEMA M2A models are that the latter used: (i) a concentrated plasticity approach to simulate beam and column behavior; and (ii) an elastic-plastic with strain hardening behavior to simulate beam behavior. Due to these minor differences, the MRSH models play an important role in this work as it serves as base of comparison for the models developed using OpenSees and the FEMA 355 models. The use of a concentrated plasticity approach or finite-length plastic hinge elements lead to negligible differences as results in Ribeiro et al. (2014) indicate.

One the MRSH modeling approach is validated, the MRB models are used in the numerical simulation carried out in this work as it is considered that the MRB models present several advantages over the MRSH model, including a more accurate simulation of nonlinear beam behavior since the bilinear models with degradation used are based on experimental calibration of the employed phenomenological laws. In addition, it is worth noting that both MRB and MRSH models developed allow for explicit consideration of the axial force-bending moment interaction for columns, which are not possible if a concentrated plasticity approach is used in modeling columns, as developed in the original FEMA 355 models.

2.3 Modeling considerations

2.3.1 Columns

Columns are modeled by considering a distributed plasticity model and an elasto-plastic constitutive law with a 3% hardening rate assigned to each fiber. A moment curvature analysis of the column section shows that this corresponds to a section hardening of approximately 3.0%, consistent with the assumptions used in the modelling for FEMA 355C (2000). Thus, for the

columns, the primary phenomenon under consideration is the interaction between moment and axial load (Ribeiro et al., 2014).

The models described in Gupta and Krawinkler (1999) correspond to concentrated plastic hinge models and use a linear axial force-bending moment (P-M) interaction surface for compressive axial loads greater than 0.15Py. While the model in FEMA (2000) considers this simplified bilinear P-M interaction surface, the P-M interaction surface considered in this study is obtained implicitly during the analysis because the columns are modeled using fiber section nonlinear beam-column elements. Similarly to the approach in FEMA 355, column splices are neglected in this study.

Columns of the consolidated frame added to the M2A models are modeled in a similar manner. However, the stress-strain relationship assigned to each fiber is modified such that the overall stiffness and strength of each column corresponds to the sum of stiffnesses of half of the overlapping interior columns (i.e., columns in each alignment), as shown in Figure 1 and Figure 2, considering the stiffness of each column calculated about the representative axis.

For 3-story buildings, consolidated frame interior columns are pinned at the base, whereas consolidated frame exterior columns and moment resisting frame columns (both exterior and interior), which are associated with the orthogonal MRF are base fixed. Otherwise, for LA9 building, both moment resisting frame and consolidated frame columns are pinned at the base.

Following the element numbering shown in Figure 1 and Figure 2, Table 5 to Table 7 show the effective column sections of the consolidated frame.

Table 5 – LA3 building - Consolidated frame effective column sections

Columns (see Figure 1)	Effective section
C1, C5, C6, C10, C11, C15	1x(W14x257* + W14x68*) + 0.5x(W14x311*)
C2, C3, C7, C8, C12, C13	1.5x(W14x82) + 1.0x(W14x68)
C4, C9, C14	2.5x(W14x68)

*weak-axis

Table 6 – SEA3 building - Consolidated frame effective column sections

Columns (see Erro! A origem da referência não foi encontrada.)	Effective section
C1, C5	1x(W14x159* + W10x77*) + 0.5x(W14x176*)
C6, C10, C11, C15	1x(W14x159* + W10x60*) + 0.5x(W14x176*)
C2-C4	2.5x(W10x77)
C7-C9, C12-C14	2.5x(W10x60)

*weak-axis

Table 7 – LA9 building - Consolidated frame effective column sections

Columns (see Figure 2)	Effective section
C1, C6, C7, C12	2x(W14x500*)
C2-C4, C8-C10	1x(W14x211) + 1x(W14x193)
C5, C11	2x(W14x193)
C13, C18, C19, C24	2x(W14x455*)
C14-C16, C20-C22	1x(W14x159) + 1x(W14x145)

C17, C23	2x(W14x145)
C25, C30, C31, C36	2x(W14x370*)
C26-C28, C32-C34	1x(W14x120) + 1x(W14x109)
C29, C35	2x(W14x109)
C37, C42, C43, C48	2x(W14x283*)
C38-C40, C44-C46	1x(W14x90) + 1x(W14x82)
C41, C47	2x(W14x82)
C49, C54, C55, C60	2x(W14x257*)
C50-C52, C56-C58	1x(W14x61) + 1x(W14x48)
C53, C59	2x(W14x48)

*weak-axis

2.3.2 Beams

For the moment resisting frame, force-based finite-length plastic hinge elements are used to model beams following the methodology proposed by Ribeiro et al. (2015) and recommendations by Scott and Ryan (2013). This approach allows for explicitly modelling the plastic hinge length and separates the behavior of the beam within the span from that of the beam-column connections. Compared to zero-length springs (used in a concentrated plasticity approach), finite-length plastic hinge elements allow faster model development as a result of the reduction in the number of nodes and elements. The plastic hinge moment-rotation behavior differs from an elastic-plastic strain hardening model (MRSH model) as it uses a bilinear (Bilin02 in OpenSees, Ribeiro et al. 2017) model with deterioration (MRB model).

The Bilin model corresponds to a modified version of the phenomenological model proposed by Ibarra and Krawinkler (2005), applicable to any force deformation relationship, is employed to simulate beam behavior and compared to a bilinear model with kinematic hardening. This model was used in Lignos and Krawinkler (2012) to model the moment-rotation relationship of plastic hinges in steel elements. The model considers strength and stiffness deterioration, as shown in Figure 5, defined in terms of element geometry, material properties, and cross-sectional geometry. Model parameters were computed based on empirical expressions proposed in Lignos and Krawinkler (2012). The Bilin model is used herein to define moment-curvature plastic hinge behavior following the implementation proposed by Ribeiro et al. (2017).

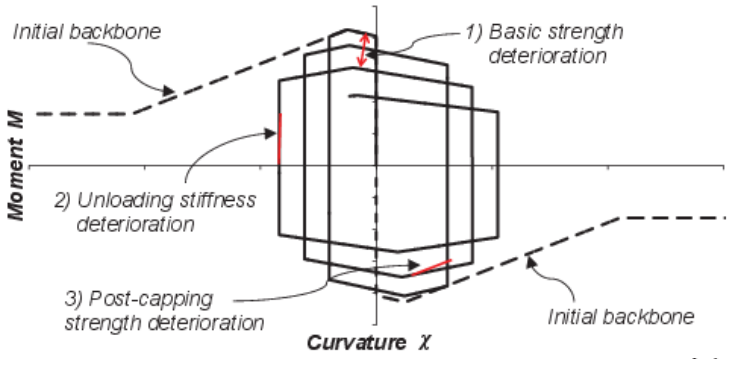

Figure 5 – Overview of the Bilin moment-curvature model that simulates beam plastic hinge behaviour.

For the buildings under analysis, the axial load expected to develop in beams is very low and the interaction between axial load and bending moment in beams is significantly less relevant than the deterioration of stiffness and strength, which is expected to occur in the beams. For this reason, the interaction between axial load and bending moment is disregarded for the beams.

In what concerns the consolidated frame, beams are modeled as elastic beam elements. This is due to the fact that in this case beam connections are simple shear connections. Note that the stiffness of the consolidated frame beams corresponds to the sum of stiffness of half of the overlapping interior beams as represented in Figure 1 and Figure 2. Following the element numbering shown in these figures, Table 8 to Table 10 show the effective beam sections of the consolidated frame.

Table 8 – LA3 building - Consolidated frame effective beam sections

Beams (see Figure 1)	Effective section
B1 - B8	2.5x(W18x35)
B9, B11, B12	2.5x(W16x26)
B10*	1.5x(W21x44) + 1.0x(W16x26)

*different due to presence of penthouse

Table 9 – SEA3 building - Consolidated frame effective beam sections

Beams (see Erro! A origem da referência não foi encontrada.)	Effective section
B1 – B8	2.5x(W16x26)
B9 – B12	2.5x(W14x22)

Table 10 – LA9 building - Consolidated frame effective beam sections

Beams (see Figure 2)	Effective section
B1 – B5	2x(W21x44)
B6 – B45	2x(W18x35)
B46, B49, B50	2x(W16x26)
B47*, B48*	1x(W21x44) + 1x(W16x26)

*different due to presence of penthouse

2.3.3 Shear Connections

Interior frames are typically designed to carry out only gravity loads. As a consequence, interior beam-to-columns connections are usually designed using shear tabs and no flange connections and treated as pin connections without bending strength. However, due to the large number of these type of connections, their contribution may be significant to the strength capacity. In this work zero-length rotational springs are used to model the equivalent strength and stiffness of all simple (shear) connections. Each spring represents the cumulative strength of half the number of overlapping simple connections in each alignment. Based on previous studies (Luco 2000 and Gupta and Krawinkler 1999) and experimental testing (Liu & Astaneh-Asl 2000), the shear connections in this study are assigned a strength of 20% of the plastic strength of the bare beam under compression and 10% under tension. The strength in positive bending is larger to account for the contribution of a slab (in compression). The elastic stiffness is obtained by setting the

elastic rotation as 0.02 rad under compression and 0.01 rad under tension. Figure 6 shows the assigned moment – rotation behavior to shear connections.

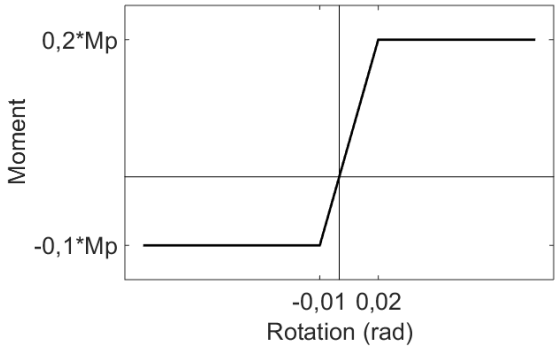

Figure 6 – Bending moment – rotation assigned to model shear connection behavior

2.3.4 Concrete deck (slab)

Previous research has proven that the interaction between the floor slab and the steel girders results in, among other effects, an increase in the strength and stiffness of the beam. However, the simulation of this effect is cumbersome. In this study, similar to FEMA 355 (FEMA 2000) and Gupta and Krawinkler (1999), the contribution of floor slab is only accounted for in: (i) the increase of beam stiffness; and (ii) the strength of shear connections (as mentioned in the previous section). According to Gupta and Krawinkler (1999) the effect of floor slabs on the strength of beams forming part of the moment resisting frame, as well as on the panel zone, is usually small and its simulation is complex.

The effective width of the floor slab for estimating the contribution to beam stiffness is calculated following the equations developed in Kato et al. (1984). It is considered that the effective stiffness under tension (slab in tension) is equal to the bare beam due to the small reinforcement in the floor slabs (typically a wire mesh). The effective moment of inertia of the composite sections varies over the span of the girder. In this model, an average of the effective inertia in compression and tension is assigned to the beam section. The stiffness of the SMRF beams has an average increase of 58% for the LA3 building, 80% for the SEA3 building, and 68% for the LA9 building.

2.3.5 Panel zones

In this model, panel zones are characterized by hysteretic behavior, including a considerable increase in strength beyond first yielding, significant cyclic hardening, and large hysteresis loops. The panel zones usually deform into a parallelogram shape. The monotonic shear force-shear distortion relationship proposed in Krawinkler (1978), which is characterized by a trilinear behavior, is used in this work to simulate the panel zone behavior. This model was also adopted by Gupta and Krawinkler (1999) and recommended in FEMA 355. This model assumes that plastic shear strength is reached at a rotation of four times the yielding rotation. Beyond this point, an appropriate value of the strain-hardening can be assumed to fully define the trilinear shear force-distortion relationship of the panel zones. Following the recommendations in Gupta and Krawinkler (1999), 3% strain-hardening is considered. Further details and a complete description of the model implemented can be found in Gupta and Krawinkler (1999). In summary, the panel

zone regions are modeled using a combination of rigid beam-column elastic elements, which form a parallelogram of dimensions d_b (depth of beam) by d_c (depth of column) and a zero-length rotational spring that simulates the trilinear shear-distortion relationship.

3 Model verification

The developed models are compared to those developed in Gupta and Krawinkler (1999), which are the FEMA 355 reference models in order to validate the modeling approach used in this study. The model validation performed includes the comparison of results for both a nonlinear static pushover and nonlinear dynamic time-history analyses. Furthermore, the building's first mode period of vibration shown in FEMA 355 also correlates well with those obtained in the finite-element models developed in this work, as shown in Table 11 to Table 13.

Table 11 – LA3 structure - First mode period of vibration using different analytical models

Model	1st Mode Period (sec)	Beam Modeling Approach
M2A FEMA355	0.850	Bilinear model with strain-hardening
M2A MRSH Model	0.862	Elastic-plastic model with strain-hardening
M2A MRB Model	0.862	Bilinear model with deterioration
M1 FEMA355	1.030	Bilinear model with strain-hardening
M1 MRSH Model	1.041	Elastic-plastic model with strain-hardening
M1 MRB Model	1.041	Bilinear model with deterioration

Table 12 – SEA3 structure - First mode period of vibration using different analytical models

Model	1st Mode Period (sec)	Beam Modeling Approach
M2A FEMA355	1.150	Bilinear model with strain-hardening
M2A MRSH Model	1.135	Elastic-plastic model with strain-hardening
M2A MRB Model	1.135	Bilinear model with deterioration

Table 13 – LA9 structure - First mode period using different analytical models

Model	1st Mode Period (sec)	Beam Modeling Approach
M2A FEMA355	1.970	Bilinear model with strain-hardening
M2A MRSH Model	1.942	Elastic-plastic model with strain-hardening
M2A MRB Model	1.942	Bilinear model with deterioration

3.4.1 Nonlinear Static Analysis

Nonlinear static analyses are performed by considering the two MRSH and MRB models. The applied lateral load pattern is proportional to the floor masses of the building as:

$$F_x = \frac{w_x h_x^k}{\sum_{i=1}^{n} w_i h_i^k} \quad (1)$$

where F_x is the normalized load at floor level x, w_x and w_i are the seismic weights at floor x and i, respectively, h_x and h_i are the heights from the ground level to floor x and i, respectively, and k is a period-dependent factor. A value of $k = 2$ is used in this study, similarl to the approach in FEMA 355c. Note that a value of $k = 1$ leads to a triangular load pattern.

Figure 7 to Figure 9 show the pushover curves, i.e. the normalized base shear (base shear normalized by structure seismic weight, or V/W) versus roof drift ratio (roof displacement normalized by structure height), for the developed models. These figures show that the pushover curves for the models with strain hardening, i.e. the FEMA 355 models and the MRSH models match well. In the elastic range, the differences between the MRSH and MRB models to the results presented by FEMA 355 are small. Such differences are expectable as a consequence, for example, of alternative beam and column modelling approaches (concentrated plasticity vs. distributed plasticity). When the bilinear model with deterioration is considered (MRB model), the post-peak force decreases as a result of the strength deterioration considered for beams, namely strain softening behavior.

In summary, the results of the pushover analysis show that the MRSH model, which uses elastic-plastic with strain hardening law for simulating beam moment-rotation response, leads to results similar to those described in FEMA 355 and Gupta and Krawinkler (1999). Second, the use of bilinear model with deterioration, i.e. MRB model, for the beams produced a larger strength reduction in the post-peak region.

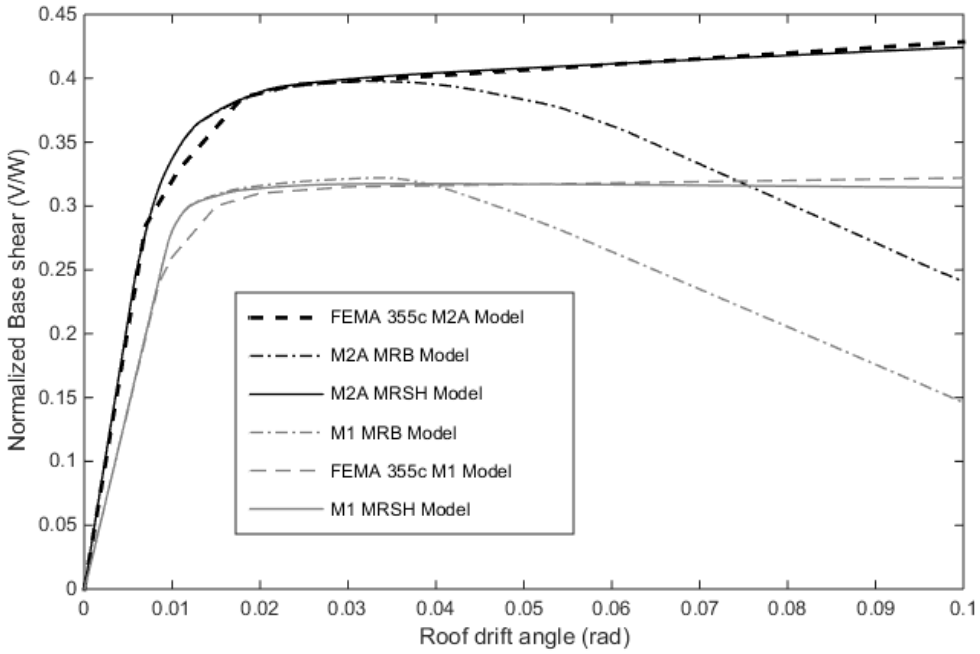

Figure 7 – LA3 building - Pushover curves obtained with MRB, MRSH, and FEMA 355 for M1 and M2A models

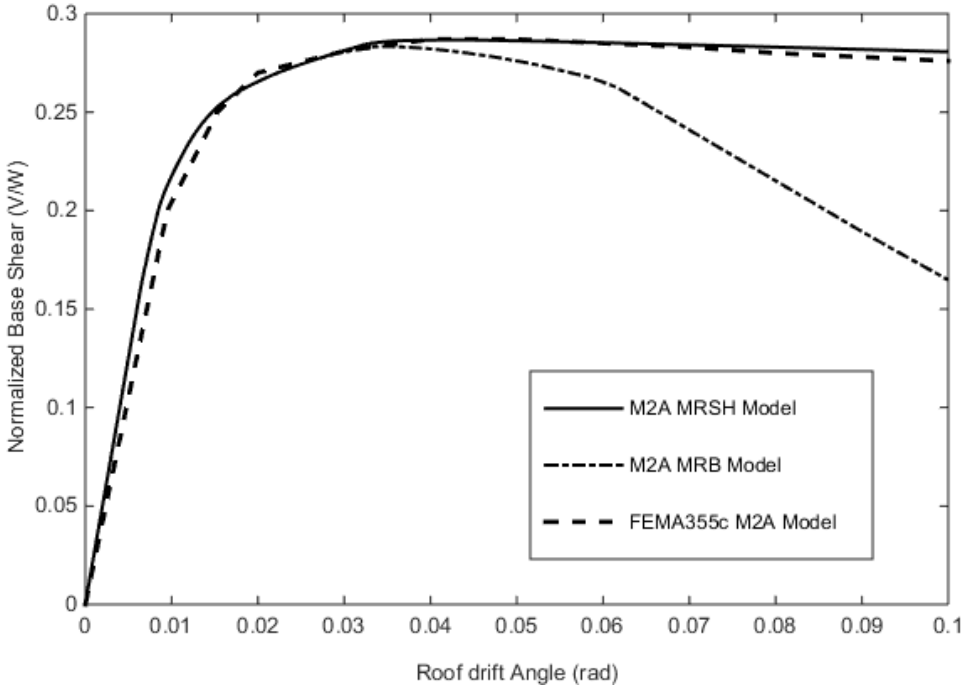

Figure 8 – SEA3 building - Pushover curves obtained with MRB, MRSH, and FEMA 355 for M2A model

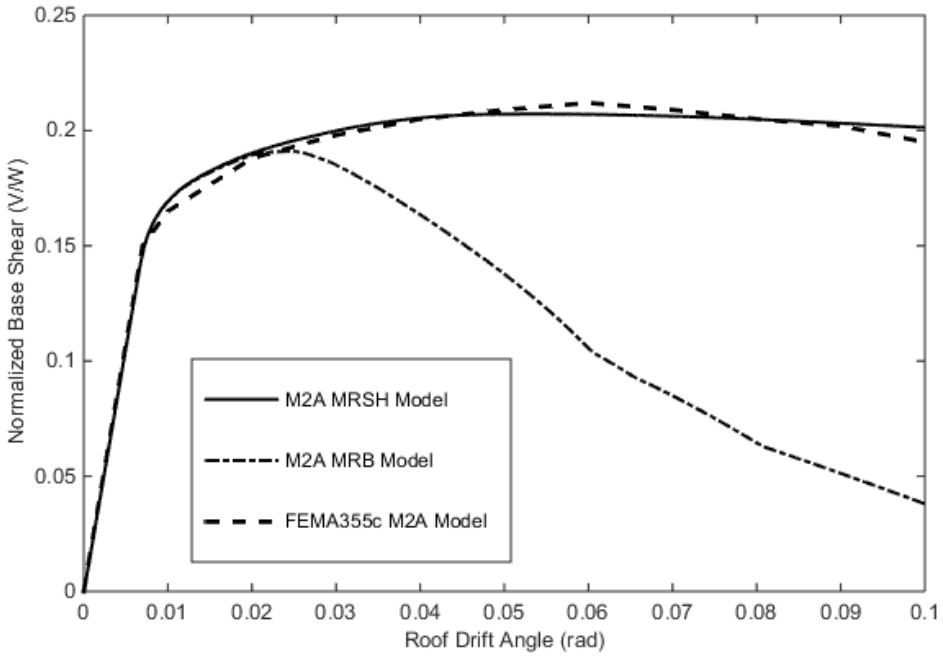

Figure 9 – LA9 building - Pushover curves obtained with MRB, MRSH, and FEMA 355 for M2A model

3.4.2 Nonlinear Dynamic Analysis

The objective of this section is to validate the developed models through comparison of the nonlinear dynamic time-history response analysis. This serves as validation for the dynamic performance of the structures and their nonlinear behavior during cyclic loading. In this context, the building models are subjected to 20 ground motions that constitute the 2/50 (2% probability of being exceeded in 50 years) hazard level set of SAC Steel Project ground motion database for Los Angeles, CA, and Seattle, WA. The roof drift ratio is considered as the main engineering demand parameter in this comparison. Similarly to the previous section, both MRSH and MRB models are analyzed in this section. Figure 10 to Figure 13 show the roof drift ratios obtained with MRSH and MRB models, as well as with FEMA 355 model, when subjected to the twenty 2/50 ground motion records. These figures show that drift ratios associated with MRB model, which is characterized by beam moment-rotation behavior that considers monotonic and cyclic deterioration, are slightly larger than those associated with MRSH model, in which beam moment-rotation behavior is described by a bilinear model with strain-hardening. The numerical analyses that lead to drift ratios larger than 0.1 rad (10%) are considered to be collapse cases. For example, in the case of the LA3 M2A building model (see Figure 10), there are five ground motion records that recorded collapse for the MRB model. However, in these same five ground motions, no collapses are recorded in MRSH model. Moreover, roof drift ratios obtained with MRSH model are generally close to those obtained with FEMA 355 M2A model, which demonstrates the validity of the developed model. In these figures, the median drift ratios of the three models are also represented in dashed lines. Note that in Figure 13 no individual results of the FEMA 355 model are available and thus are not represented in this figure.

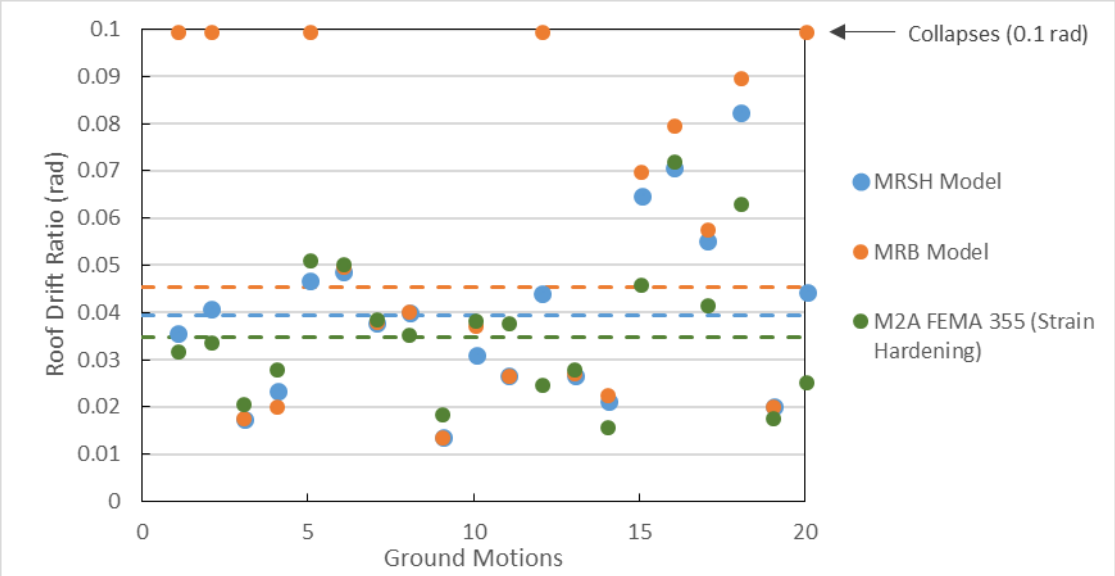

Figure 10 – LA3 building - Nonlinear dynamic analysis - roof drift ratio obtained with models MRSH and MRB, as well as with FEMA 355c M2A model, under the SAC 2/50 ground motion set

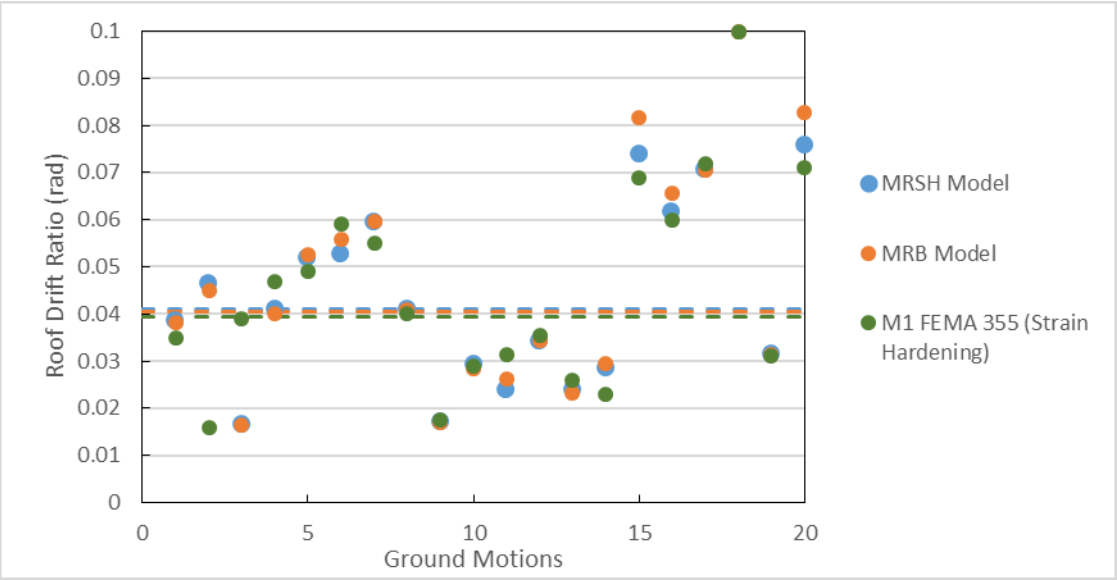

Figure 11 – LA3 building - Nonlinear dynamic analysis - roof drift ratio obtained with models MRSH and MRB, as well as with FEMA 355c **M1** model, under the SAC 2/50 ground motion set

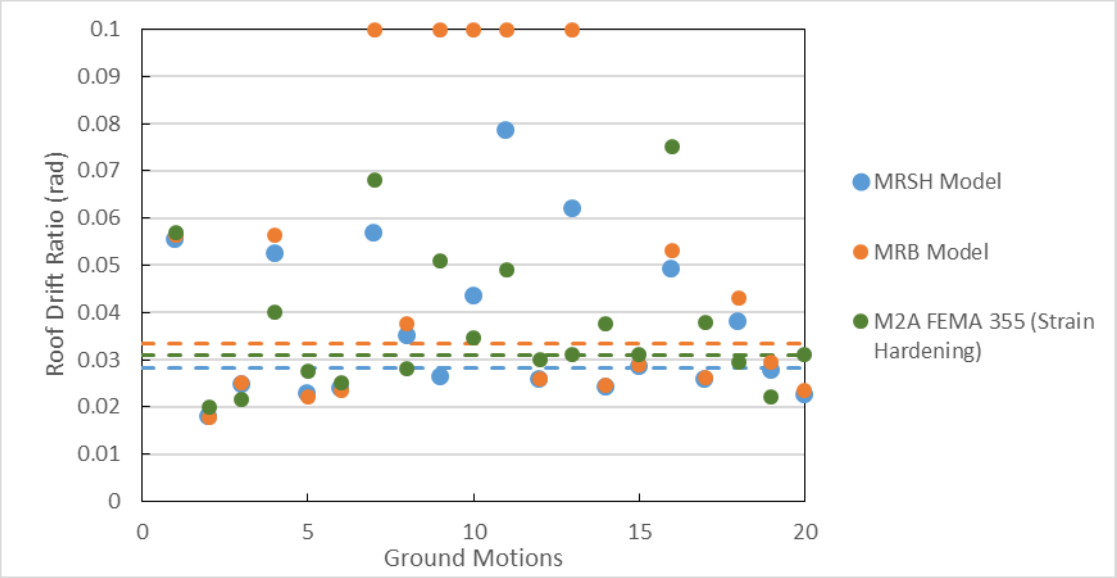

Figure 12 – SEA3 building - Nonlinear dynamic analysis - roof drift ratio obtained with models MRSH and MRB, as well as with FEMA 355c **M2A** model, under the SAC 2/50 ground motion set

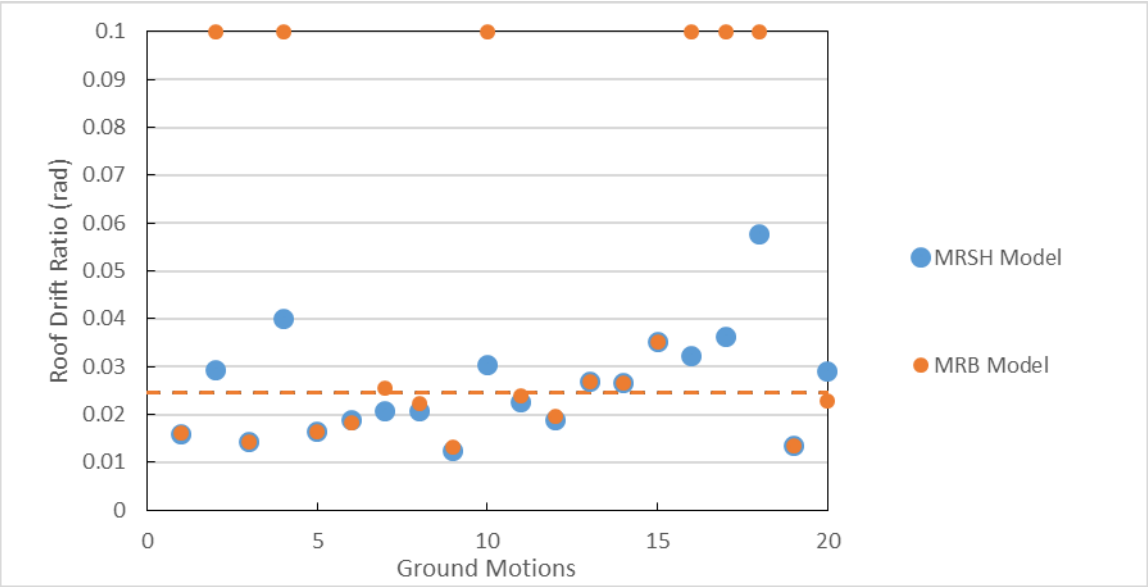

Figure 13 – LA9 building - Nonlinear dynamic analysis - roof drift ratio obtained with models MRSH and MRB, as well as with FEMA 355c **M2A** model, under the SAC 2/50 ground motion set

As a conclusion, Table 14 to Table 16 summarize results obtained in the performed nonlinear dynamic analysis, namely median, maximum, minimum, as well as the 84th percentile. The results of the FEMA 355 models are shown for comparison purposes.

Table 14 – LA3 building - Statistical values of roof drift ratio (in rad) for different analytical models subjected to SAC 2/50 ground motion set

Roof Drift Ratio (rad)	FEMA 355 M2A Model	M2A MRSH Model	M2A MRB Model	FEMA 355 M1 Model	M1 MRSH Model	M1 MRB Model
Median	0.0339	0.0388	0.0455	0.0401	0.0410	0.0405
Minimum	0.0167	0.0145	0.0140	0.0168	0.0165	0.0164
84th Percentile	0.0511	0.0556	0.1000	0.0657	0.0703	0.0702
Maximum	0.0734	0.0785	0.1000	0.1000	0.1000	0.1000

Table 15 – SEA3 building - Statistical values of roof drift ratio (in rad) for different analytical models subjected to SAC 2/50 ground motion set

Roof Drift Ratio (rad)	FEMA 355 M2A Model	M2A MRSH Model	M2A MRB Model
Median	0.0310	0.0282	0.0335
Minimum	0.0200	0.0178	0.0178
84th Percentile	0.0506	0.0547	0.1000
Maximum	0.0750	0.0785	0.1000

Table 16 – LA9 building - Statistical values of roof drift ratio (in rad) for different analytical models subjected to SAC 2/50 ground motion set

Roof Drift Ratio (rad)	FEMA 355 M2A Model	M2A MRSH Model	M2A MRB Model
Median	0.0237	0.0246	0.0246
Minimum	0.0107	0.0125	0.0132
84th Percentile	0.0358	0.0351	0.1000
Maximum	0.0551	0.0577	0.1000

This comparison is considered sufficient for dynamic analysis validation of the MRSH model. Although no direct validation of the MRB model is possible, the definition of component degradation is consistent with experimental results and P-M interaction is explicitly considered. Considering the advantages of the described finite length model and including realistic effects of the deterioration of beam properties in the analysis, the MRB model is used in the fragility analysis.

References

Allahabadi, R. and Powell, G. (1988). "DRAIN-2DX user guide", Report No. UCB/EERC-88/06, Earthquake Engineering Research Centre (EERC), University of California at Berkeley

Erduran, E. (2012). "Evaluation of Rayleigh damping and its influence on engineering demand parameter estimates." Earthquake Eng. Struct. Dyn., 41(14), 1905–1919.

FEMA. (2000). "State of the art report on systems performance of steel moment frames subjected to earthquake ground shaking." FEMA-355C, Washington, DC.

Gupta, A., and Krawinkler, H. (1999). "Seismic demands for performance evaluation of steel moment resisting frame structures." Rep. No. 132, John A. Blume Earthquake Engineering Center, Stanford, CA.

Ibarra, L. F., and Krawinkler, H. (2005). "Global collapse of frame structures under seismic excitations." Rep. No. 152, John A. Blume Earthquake Engineering Research Center, Dept. of Civil Engineering, Stanford University, Stanford, CA.

International Conference of Building Officials (ICBO). (1994). "Structural engineering design provisions." Uniform building code, Vol. 2, Whittier, CA.

Kato, B., Aoki, H., and Tagawa, Y. (1984). "Seismic behaviour of steel frames with composite girders", Proc. 8th World Conference on Earthquake Engineering, San Francisco, Vol. VI.

Krawinkler, H. (1978). "Shear design of steel frame joints", Engineering Journal, AISC, Vol. 15, No.3.

Liu, J. and Astaneh-Asl, A. (2000), "Cyclic testing of simple connections including effects of slab," *ASCE Journal of Structural Engineering*, 126(1): 32-39.

Lignos, D., and Krawinkler, H. (2012). "Development and utilization of structural component databases for performance-based earthquake engineering." J. Struct. Eng., 10.1061/(ASCE)ST.1943-541X.0000646, 1382–1394.

Luco, N. and Cornell, A.C. (2000). "Effects of Connection Fractures on SMRF Seismic Drift Demands", Journal of Structural Engineering, 126:1(127).

OpenSees, Version 2.5.0 [Computer software]. Berkeley, CA, Pacific Earthquake Engineering Research Center.

Scott, M. H., and Fenves, G. L. (2006). "Plastic hinge integration methods for force-based beam-column elements." J. Struct. Eng., 10.1061/ (ASCE)0733-9445(2006)132:2(244), 244–252.

Scott, M., and Ryan, K. (2013). "Moment-rotation behavior of force-based plastic hinge elements." Earthquake Spectra, 29(2), 597–607.

Ribeiro, F., Barbosa, A., Scott, M., and Neves, L. (2015). "Deterioration Modeling of Steel Moment Resisting Frames Using Finite-Length Plastic Hinge Force-Based Beam-Column Elements." J. Struct. Eng., 141(2), 04014112.

Ribeiro, F., Neves, L., and Barbosa, A. (2017). "Implementation and calibration of finite-length plastic hinge elements for use in seismic structural collapse analysis." Journal of Earthquake Engineering*, doi: 10.1080/13632469.2015.1036327.*